Chapter 2

Advanced Fabrication and Characterization of Magnetic Nanowires

Hanan Mohammed, Julian A. Moreno and Jürgen Kosel

Additional information is available at the end of the chapter

http://dx.doi.org/10.5772/intechopen.71077

Abstract

Magnetic nanowires feature unique properties that have attracted the interest of different research areas from basic physics over biomedicine to data storage. The combination of crystalline and shape anisotropy is mainly responsible for the magnetic properties of the nanowires, whereby different methods for tuning those properties are available. The nanowires typically represent single-domain particles, and magnetization switching occurs via domain walls nucleated at the ends of the nanowire and traversing it. Combined with a high biocompatibility, iron or iron oxide nanowires can be used as nanorobots for biomedical applications, destroying cancer cells, or delivering drugs. The nanowires are also attractive for data storage, especially in a three-dimensional device, because of the high-domain wall speed that has been theoretically predicted. This chapter offers an introduction to the electrochemical synthesis of cylindrical nanowires in anodic aluminum oxide (AAO) templates. Template modification techniques such as barrier layer thinning, barrier layer etching, and diameter modulation are discussed. Advanced fabrication techniques of nanowires with varying structural and chemical variations such as multisegmented and core-shell nanowires are elaborated. The characterization of single nanowires encompassing physical, magnetic, and electrical techniques is covered.

Keywords: nanotechnology, nanofabrication, magnetic nanowires, cylindrical nanowires, anodic aluminum oxide templates, anodization, diameter modulated nanowires, core-shell nanowires, multisegmented nanowires, single nanowire characterization, single nanowire electrical contacting

1. Introduction

Cylindrical magnetic nanowires are novel materials that offer unique properties, mainly due to a high aspect ratio and shape anisotropy. They are typically characterized by a single

magnetic domain, rendering them permanent magnetic. This feature allows utilizing such nanowires as remotely operated nanorobots, i.e., induce motion, produce heat, or sense their location. This makes them attractive for numerous applications like flow sensors [1], magnetic separation [2], bio-inspired tactile sensors [3], energy harvesting [4], cancer treatment [2, 5], drug delivery [6, 7], and MRI contrast agent [2, 8]. Nanowires are also used for other applications such as magnetic force microscopy (MFM) tips [9], giant magnetoresistance (GMR) [10], spin transfer torque (STT) [11, 12], and data storage devices [13–15].

In order to exploit these nanowires to their full advantage, a reproducible fabrication method is required that yields nanowires of high quality and specific properties. Electrodeposition of nanowires into templates is such a method and is described in more detail. The properties of magnetic nanowires can be tailored in different ways to optimize them for particular applications. For instance, multisegmented nanowires and core-shell nanowires will be discussed below, which allow combining the properties of several materials. This can result in e.g., large magnetization values in combination with high biocompatibility, as will be shown below.

On the other hand, characterizing these properties is a crucial task for the magnetic behavior of the nanowires and the influence of different parameters. The magnetic properties of nanowires have typically been measured for large numbers of nanowires arranged in arrays inside the templates, which provide large signals but compromise the information content. More recently, individual nanowires were characterized with magnetic force, magneto-optical Kerr effect, and electron microscopy methods as well as magneto resistivity. In this chapter, we will focus on single nanowire characterization methods and results, which provide much deeper insight into the magnetic and structural details of the nanowires. Further understanding can be obtained, when the experimental results are combined with micromagnetic simulations, which conveniently allow varying parameters.

2. Anodic aluminum oxide as nanowire templates

Electrochemical deposition into nanostructured templates represents a widespread and inexpensive bottom up approach for the fabrication of metallic nanowires with a high aspect ratio and high pore density [16–18]. Anodic aluminum oxide (AAO) templates have emerged as a popular template, due to their versatile fabrication technique, wherein the pore diameter, length, and inter pore distances can be tuned with ease. The AAO templates are relatively easy to make in-house with low costs and scalable processing. In addition to obtaining vertically aligned nanopores, modifying the template fabrication process can yield diameter-modulated nanopores [19, 20].

2.1. Mechanism of anodic aluminum oxide template formation

Self-ordered pores organized in a close-packed hexagonal lattice are obtained by anodic oxidation of aluminum (mild anodization) in a suitable acidic environment such as sulfuric, oxalic, or phosphoric and under appropriate electrolyte conditions such as pH, concentration, and temperature [21–25]. The AAO template formation or anodization proceeds with the conversion of the naturally occurring preexisting oxide film on the aluminum surface into a thicker oxide layer referred to as a planar barrier-type film (**Figure 1(1)**). The planar barrier-type film converts into a porous oxide layer by forming random cracks in the outer regions of the barrier oxide layer (**Figure 1(2)**), which

further forms individual pathways until a steady-state pore structure is created (**Figure 1(3)**). Once a steady state is achieved, pores proceed throughout the anodized material (**Figure 1(4)**).

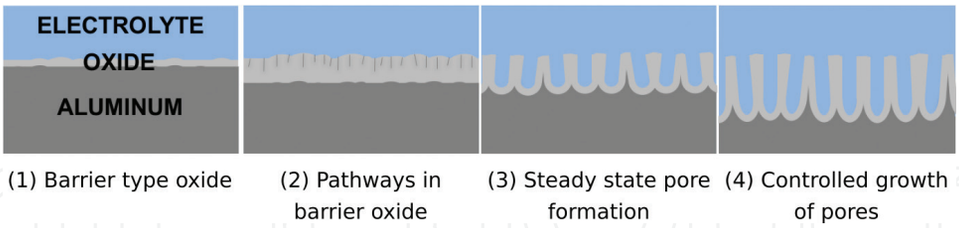

Figure 1. Mechanism of anodic aluminum oxide template formation. (1) Formation of barrier type oxide layer, (2) pathways created in the barrier oxide layer, (3) steady state formation of pores, (4) controlled growth of nanopores.

Since pore formation is initiated at random locations on the aluminum surface, an ordered pore arrangement can be obtained by the fabrication of dimples in the aluminum at the intended position of the pores. The dimples can be fabricated by direct indentation such as with the tip of a scanning probe microscope [26–28], milling with a focused ion beam [28, 29], or nanoindentation using Si_3N_4 [30] or Ni [31] stamps. An easy alternative approach for pore ordering is the two-step anodization or double anodization method developed by Masuda and Fukuda based on self-organization [21]. It is this double anodization method that has attracted much interest for AAO to be used as nanowire templates as well as for many other applications. The porous oxide film formed after an anodization process (first anodization) is poorly ordered with varying pore diameters and inter pore distances at the top surface but has a high degree of order at the bottom of the pores (**Figure 2(1)**). In the double anodization method, the first porous oxide layer is chemically removed (**Figure 2(2)**) to reveal semi-spherical etch pits or dimples (**Figure 2(3)**) that are highly ordered and uniform. A second anodization process is

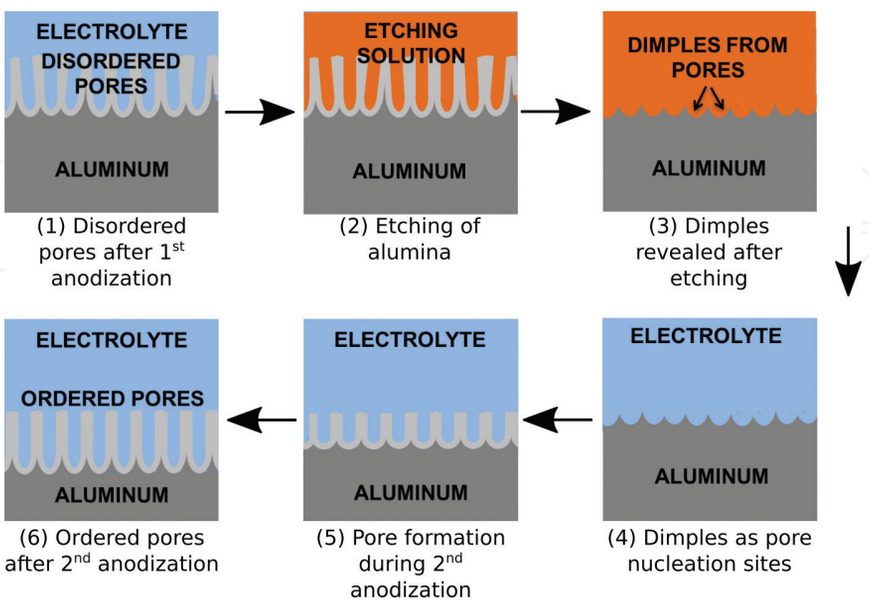

Figure 2. Mechanism of double anodization process. (1) Disordered pores formed after the first anodization step, (2) alumina layer is etched, (3) etching reveals dimples on the aluminum template, (4) the dimples serve as pore nucleation sites for a second anodization process, (5) formation of ordered pores during second anodization, (6) ordered pores obtained after second anodization.

performed, wherein the dimples serve as the pore nucleation sites (**Figure 2(4)**), and the subsequent pores grow exactly on the dimples (**Figure 2(5)**). Thus, the first anodization itself is used as the prepatterning step. Since anodization is a faradic process, the longer the anodization process, the longer will be the pores. Also, longer anodization times result in improved pore ordering, wherein the best pore ordering exists at the bottom of the AAO pores, i.e., the layer that was grown last (**Figure 2(6)**).

2.2. Fabrication of diameter-modulated templates

A diameter-modulated cylindrical nanowire refers to a nanowire, which possesses a changing diameter along its length. Such nanowires can be obtained by using diameter-modulated alumina templates, which are prepared through a combination of *hard* and *mild* anodization processes [19, 32, 33]. Mild anodization of aluminum was described in Section 2.1 and is constrained to very tight equilibrium regimes (voltage, temperature, concentration, and stirring) at which highly ordered, well-defined pores with fixed diameter and inter pore distance are obtained. Deviations from those regimes lead to lack of ordered pores or high current density flowing through the oxide layer, due to high voltages (burning) of the sample. However, the self-ordering pore regimes can be obtained at high voltages with the same concentration of e.g., oxalic acid, provided low temperatures and a starting thick oxide layer. This high voltage anodization is referred to as hard anodization, and in both cases (hard and mild), the anodization current represents a measure of the effective electric field at the oxide layer, and its value is related to the movement of ionic species through the electrolyte/oxide/metal interfaces, the oxygen ions from the electrolyte being the limiting factor [34, 35]. Because of the high-applied voltage in hard anodization, the electric field at the oxide/metal interface results in a continuously increasing thickness of the oxide layer, limiting the length of ordered pores by building up internal stresses, due to the volume expansion. In order to produce diameter modulations, two main approaches can be used: a combination of mild anodization in phosphoric acid (high diameter) and hard anodization in oxalic acid (low diameter), changing solutions in each step, as in [34] or using pulsed [36] or cyclic [37] anodization on the same solution. When using the same solution, hard anodization voltages would yield a higher diameter pore than mild anodization ones. This is due to the faster dissolution of the oxide layer driven by the higher electric field, compared to lower (mild) anodization voltages [35]. Another approach to fabricate diameter-modulated templates is by chemical widening of the pores after a segment of plated metal has been deposited in a nonmodulated anodized template [38].

A general diameter modulation of an alumina template, using pulsed or cyclic anodization, would proceed as in **Figure 3**. After electropolishing the aluminum disc, mild anodization is performed to form a first thick oxide layer (**Figure 3(a)**). This reduces the effective electric field at the oxide layer when higher voltages are applied, limiting the production of high current densities from *burning* the sample. Then, the voltage is slowly increased (0.05–0.5 V/s) until it reaches the hard anodization value (**Figure 3(b)**). At this point, cycles between hard (high diameter) and mild (low diameter) anodization voltages can be repeated to achieve the desired pore length (**Figure 3(c)**).

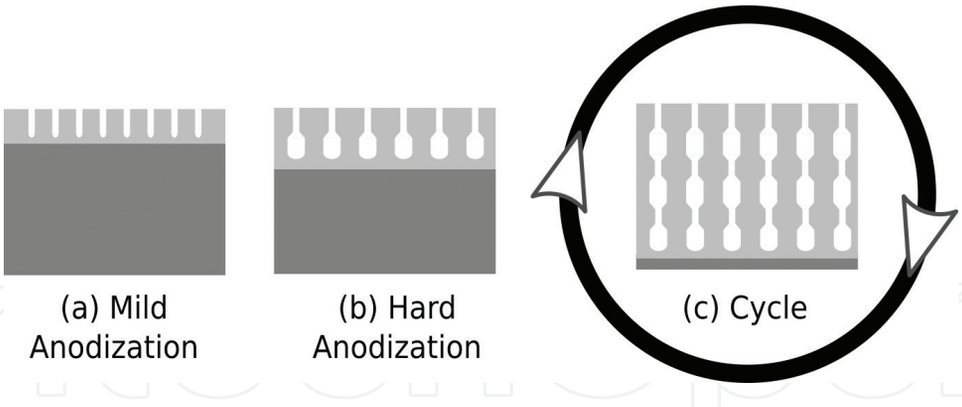

Figure 3. Diameter modulation of an alumina template. (a) Mild anodization process is carried out to create a thick oxide layer to withstand the high voltages of hard anodization, (b) voltage is slowly increased until the hard anodization voltage is reached, (c) changing the voltage from hard to mild anodization values results in the diameter modulation.

3. Electrochemical synthesis of nanowires

Electrochemical deposition or electrodeposition is an inexpensive and widely exploited technique for the deposition of metals through the chemical reduction of metal ions from an aqueous electrolyte [39]. Electrodeposition into AAO templates yields cylindrical nanowires that grow in a bottom-up fashion. The electrodeposition setup consists of an AAO template placed in contact with a cathode, and an anode placed parallel to it in an aqueous electrolyte consisting of the precursor material. Upon the application of an electric field, cations of conductive material diffuse toward the cathode and are reduced therein, resulting in the growth of nanowires inside the AAO pores whose length is monitored by the charge density during deposition. There are two common techniques to deposit nanowires namely direct current (DC) deposition and pulsed deposition. In order to perform electrodeposition, a conductive pathway should exist between the electrolyte and the cathode, but the AAO template obtained after the second anodization process lacks this feature. To overcome this problem, two approaches exist namely barrier layer removal by voltage control [18, 40] and barrier layer removal by chemical etching. The former approach results in aluminum-supported AAO templates, whereas the latter results in free-standing AAO templates.

3.1. Fabrication of nanowires in aluminum-supported aluminum oxide template templates

In the case of barrier thinning approach, the barrier layer formed after the second anodization (**Figure 4(1)**) is reduced by applying a decreasing voltage in successive steps. This process results in the formation of small root-like pathways or dendrites at the bottom of the hemispherical pores (as seen in **Figure 4(2)**), along with the thinning of the alumina barrier layer [41]. The thinned barrier layer along with the dendrites creates a lower potential for the deposition current to tunnel through the alumina barrier layer during the subsequent

electrodeposition step (**Figure 4(3)**). The deposition into aluminum supported AAO templates is a straightforward process, as it does not involve any chemical etching post-anodization, unlike the free-standing templates (Section 3.2). The pulsed deposition technique is utilized in these templates, in order to avoid charging of the barrier layer and ensure a uniform deposition of the nanowires. The pulsed deposition consists of applying a negative current pulse which attracts the positive metal ions to the bottom of the AAO pores, followed by a positive voltage pulse which discharges the alumina barrier layer. Finally, a recovery time, wherein neither a current nor a voltage pulse is applied, aids in refreshing the solution at the bottom of the pores.

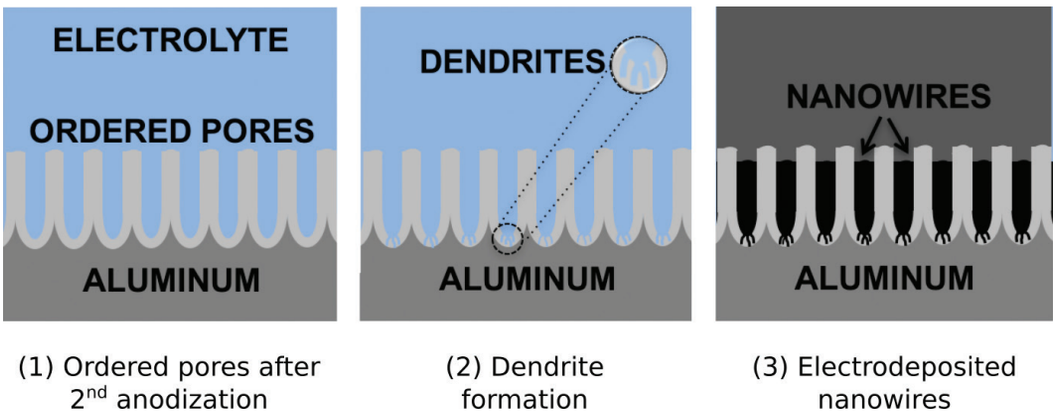

Figure 4. Electrodeposition into an aluminum supported AAO template. (1) Ordered pores after second anodization, (2) barrier layer thinning by voltage reduction resulting in the formation of dendrites, (3) electrodeposition of nanowires.

3.2. Fabrication of nanowires in free standing aluminum oxide templates

In order to obtain a free-standing template, i.e., consisting of pores open from both sides, after the second anodization (**Figure 5(1)**), the nonoxidized aluminum is removed by chemical etching under constant stirring (**Figure 5(2)**). Once the aluminum layer is removed, the alumina layer consisting of nanopores is chemically etched using an aqueous solution (**Figure 5(3)**), thereby resulting in open-ended nanochannels (**Figure 5(4)**). A conducting pathway for the electrodeposition step is achieved by physical vapor deposition of a suitable metal such as gold on the backside of the template to act as an electrode (**Figure 5(5)**). The template is then immersed in the suitable electrolyte (**Figure 5(6)**), and electrodeposition is then performed (**Figure 5(7)**) Once the electrodeposition is completed, the template is rinsed and dried (**Figure 5(8)**), and finally, the electrode is removed by plasma etching. Even though the free-standing templates are not straight forward to fabricate in comparison with the aluminum-supported AAO templates, their pores can be chemically widened, thereby providing more diameter flexibility to the AAO templates postfabrication. In addition to this, DC deposition can be performed due to the good electrical contact between the AAO template and the cathode.

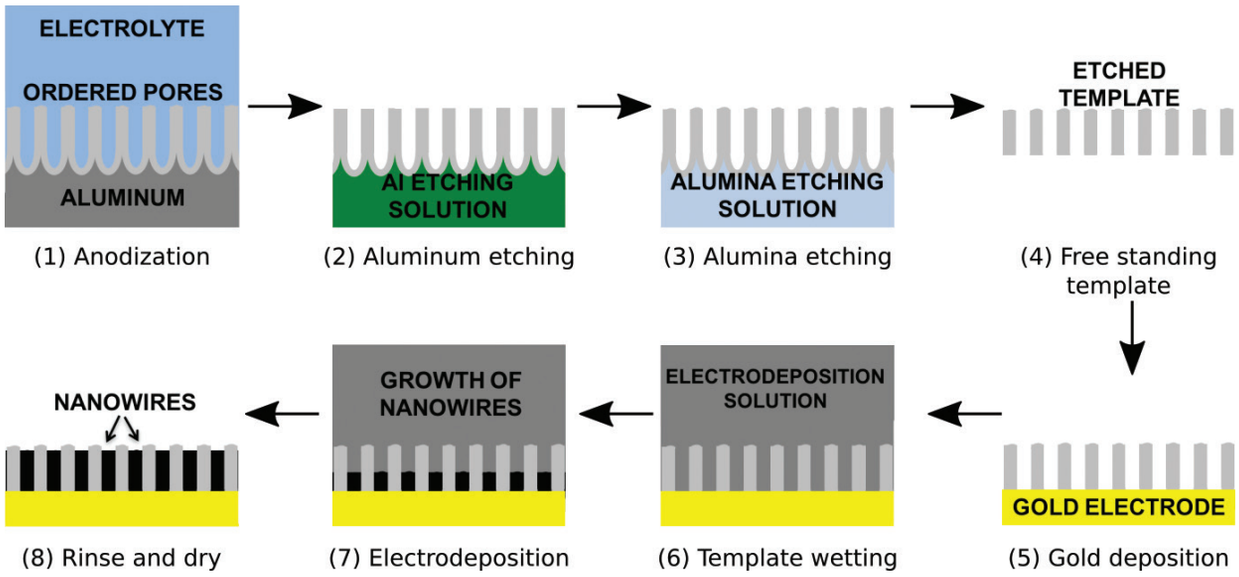

Figure 5. Electrodeposition into free-standing AAO template. (1) Ordered nanopores obtained after second anodization, (2) chemical etching of aluminum layer, (3) chemical etching of alumina layer, (4) free standing AAO template obtained, (5) electrode deposited onto the AAO template, (6) wetting the template with the electrodeposition solution, (7) electrodeposition of nanowires, (8) electrodeposited nanowires.

3.3. Fabrication of multisegmented nanowires

Multisegmented magnetic nanowires can be used for a wide range of applications such as data storage by using multisegmented Co/Ni nanowires [15, 42], functionalization, and release of molecules [43, 44], cell detection [43], etc. Multisegmented nanowires can be fabricated by electrodeposition into AAO templates using either a single electrolyte solution or more than one electrolyte solutions [15, 45–47]. In the case of a single electrolyte solution, each component within the electrolyte will have differing concentrations and deposition voltages, and alternating between the voltages will result in a multilayered structure. Since both applied voltages have the same sign, what prevents the deposition of both materials at the same time is the difference in concentration. Thus,

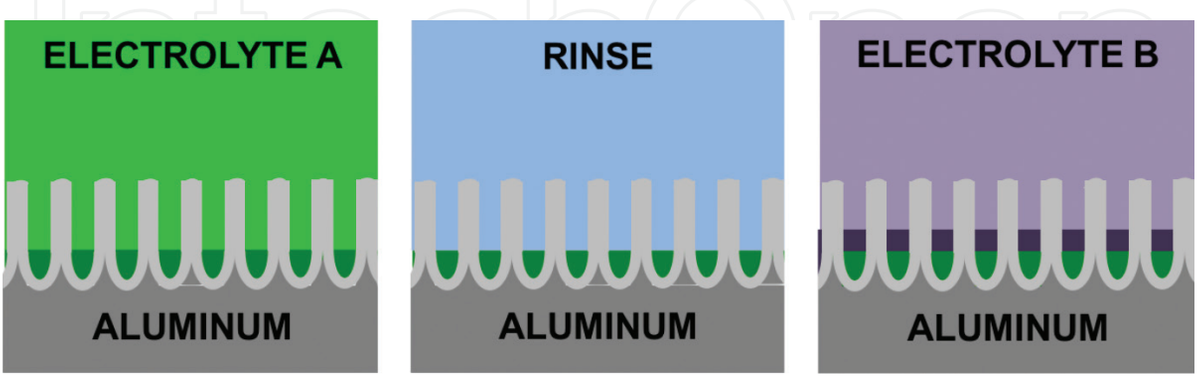

Figure 6. Electrodeposition of multisegmented nanowires using two electrolyte solutions. (1) Deposition of metal using electrolyte A, (2) rinsing of the nanopores, (3) deposition of metal using electrolyte B.

the lower concentration component will be limited by diffusion, when the higher concentration component is being deposited. If different electrolyte solutions are used, after depositing one metal (**Figure 6(1)**), the AAO template is rinsed (**Figure 6(2)**), and the second electrolyte is used for the next deposition (**Figure 6(3)**). This can be repeated several times to obtain a specific number and arrangement of segments [15].

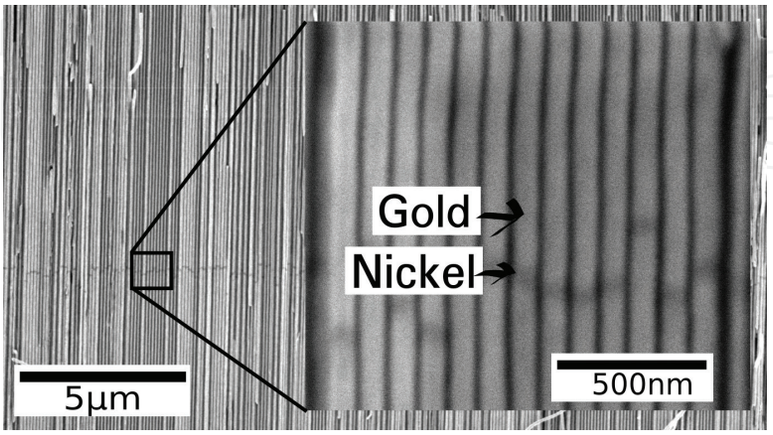

Figure 7. Scanning electron microscopy (SEM) image of a cross-section of an AAO template with multisegmented Au/Ni/Au nanowires. Inset depicts magnified image (reprinted with permission from Moreno [48] copyright 2016 KAUST).

Figure 7 depicts an example of electrodeposition using separate nickel and gold electrolyte solutions with a rinse step in between solution changes. The different contrast exhibited by the nickel segment assists in identifying different composition variation along the nanowire. The variation of the thickness of the nickel segment between different nanowires is a consequence of slight pore diameter variations within the AAO template.

3.4. Fabrication of core-shell nanowires

Core-shell nanowires consist of different core and shell materials such as metal-nonmetal or metal-metal nanowires [49–51]. They are fabricated in order to tune their magnetic properties and take advantage of the combined properties of the core and shell materials [52, 53]. One technique for realizing core-shell nanowires is by utilizing atomic layer deposition (ALD) to fabricate a shell structure. ALD is performed on AAO templates and the thickness of the deposited film is tuned by the number of ALD cycles. Once the shell structure is obtained, the core is fabricated by electrodeposition of the required material. Even though ALD can provide a conformal shell structure, the technique is an expensive as well as challenging process due to the high aspect ratio of the templates. A facile low-cost technique for fabricating metal-oxide core-shell nanowires such as iron-iron oxide (magnetite) nanowires is by oxidizing released iron nanowires in an oven at 150°C, for 10 min to 72 h in an ambient atmosphere (**Figure 8**) [50]. This technique easily allows the tuning of the geometry (such as core radius, shell thickness, and length) and crystallinity (single or polycrystalline core) of the nanowire. Consequently, the magnetic properties can be tuned, i.e., the saturation and remanence magnetization decrease with increasing shell thickness.

http://dx.doi.org/10.5772/intechopen.71077

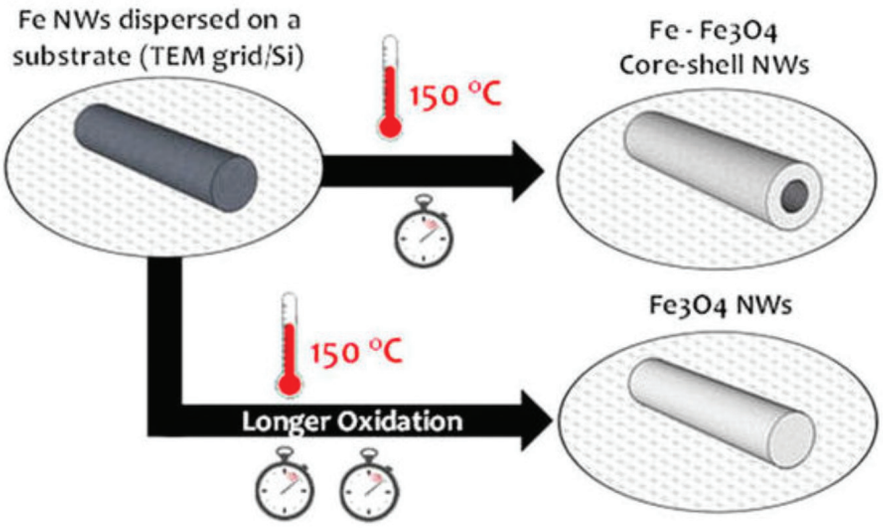

Figure 8. Fabrication process of core-shell Fe-Fe_3O_4 nanowires [18].

4. Characterization of single nanowires

A comprehensive characterization of nanowires is crucial toward utilizing these novel structures for various applications such as biosensors, drug delivery, data storage, etc. Mostly, the collective behavior of nanowires in an array has been studied [54–56], which provides some insight into the magnetic properties of the nanowires but is affected by magnetostatic interactions between them. Hence, single nanowire characterization is desirable, but there are various challenges associated with it, due to the nanowire's small dimensions. For example, the high aspect ratio of the nanowires makes it prone to mechanical deformations during their release from the template as well as during subsequent characterization. The small volume of the nanowire makes magnetic and electrical characterization challenging, due to the low magnetic signal associated with it, as well as its sensitivity to electrical discharges resulting in melting the nanowire. The characterization of single nanowires can be broadly divided into physical, magnetic, and electrical characterization. In this chapter, an overview of the various techniques for single nanowire probing is discussed.

For probing single nanowires, firstly the nanowires have to be released from the AAO template. The nanowires are released by dissolving the alumina using a selective chemical etchant. The process of release varies between nanowires in aluminum-supported AAO templates and free-standing templates with an electrode back layer. The nanowires in the aluminum-supported AAO templates are released by placing the electrodeposited AAO template in a micro centrifuge tube with a solution of sodium hydroxide at room temperature [5]. This dissolves part of the alumina resulting in the detachment of the aluminum back layer, which is then removed from the tube. To further dissolve the alumina, sodium hydroxide at room temperature or a solution of chromium oxide and phosphoric acid at around 40°C is used. Once the alumina is completely etched, the nanowires, which are now suspended in the etchant, are extensively rinsed and stored in high-purity ethanol. The ethanol rinsing is performed by

placing the micro centrifuge tube in a magnetic tube holder rack. The nanowires fabricated using the free-standing AAO templates do not possess an aluminum back layer but instead an electrode usually gold is present, which can be easily removed by ion milling. The AAO template is then chemically etched using either sodium hydroxide or a solution of chromium oxide and phosphoric acid, as described previously. The etchant concentrations, temperatures, and times may vary depending on the goal of the characterization studies [57].

4.1. Physical characterization

The geometry, morphology, chemical, and structural characteristics of single nanowires have been widely studied using electron microscopy techniques such as scanning electron microscopy (SEM) and transmission electron microscopy (TEM) [58]. For investigation under an electron microscope, the released nanowires are dispersed onto a substrate such as silicon (**Figure 9(a,b)**) or TEM grid (**Figure 9(c,d)**). The SEM is generally utilized to probe the nanowire dimensions and structural variations along its length. The SEM is particularly useful in magnifying features such as dendrites, which are present at one end of the nanowire, when they are fabricated using the aluminum-supported AAO template (**Figure 3(1)**). **Figure 9(b)** depicts the SEM image of such a nanowire (polycrystalline fcc nickel nanowire) with a relatively smooth topography, which constitutes two parts: the main part, which is cylindrical and an additional dendritic region [41]. A dendrite typically consists of two to four root-like structures of approximately 500 nm length and a slightly varying shape from one nanowire to another. The TEM on the other hand provides a high-resolution image and more detailed morphological information such as surface roughness (**Figure 9(c)**). The TEM allows imaging of the cross-sectional shape of the nanowire, which is ideally expected to be cylindrical, but in some cases, it deviates from the ideal structure (**Figure 9(d)**). This deviation is a consequence of noncircular pore shapes in the AAO template. Both SEM and TEM can provide information on the chemical composition of the nanowire using techniques such as energy-dispersive X-ray spectroscopy (EDS) [59] and electron energy loss spectroscopy (EELS) [60]. Even though the EDS technique can be performed in an SEM, its resolution is limited to identifying the presence or absence of an element, whereas EDS mapping in a TEM provides a higher spatial resolution. In comparison to the EDS, the EELS technique is a challenging technique performed using a TEM but provides a more detailed chemical mapping of the nanowire.

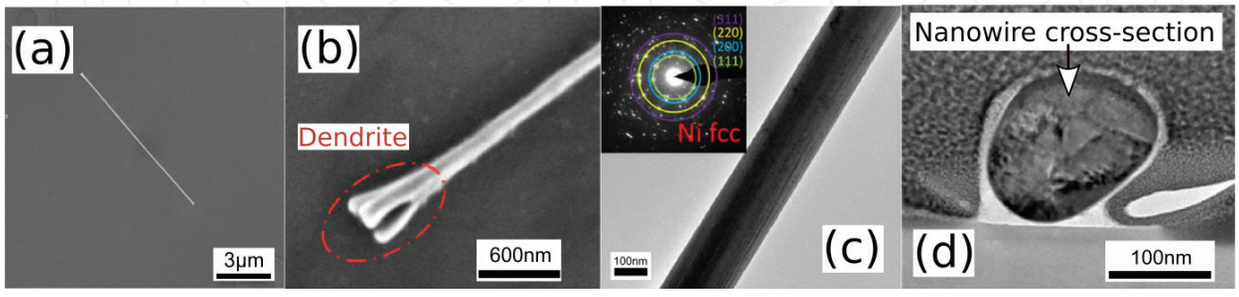

Figure 9. SEM image of a (a) nickel nanowire, (b) magnification of the end of the nanowire depicting the dendritic portion. TEM image of (c) a nickel nanowire with inset of SAED image depicting fcc structure, (d) cross-section of a nickel nanowire (reprinted from Vilanova Vidal et al. [41], with the permission of AIP publishing).

The crystalline structure of a nanowire can be probed using an electron diffraction technique referred to as selected area electron diffraction (SAED) [59]. This powerful technique offers structural information from even a small region of the nanowire. In addition to this, defects such as planar defects can be probed using dark-field TEM.

4.2. Magnetic characterization

Magnetic characterization of single nanowires yields fundamental information such as the saturation magnetization, coercivity, switching field, squareness of individual nanowires, magnetization reversal process, and the types of domain walls involved, as well as the propagation of domain walls within the nanowire. Even though the small nanowire volume makes magnetic characterization challenging due to the low magnetic signal, as well as proper positioning and orientation of the magnetic field with respect to the nanowire axis, various techniques such as magnetometry and microscopy allow the magnetic probing of individual nanowires.

4.2.1. Magnetometry

Magnetometry techniques such as super conducting quantum interference device (SQUID) and magneto-optical Kerr effect microscopy (MOKE) give an insight into the magnetic behavior of a nanowire by the acquisition of a magnetic hysteresis loop. The SQUID magnetometer, which is commonly used for nanowire array characterization, can be modified by lithographically patterning a micro-SQUID detector around a single nanowire in order to sense the low magnetic signal arising from a single nanowire [13, 61]. By measuring the hysteresis curves along the axial and transverse directions, the easy axis of the nanowire can be easily determined. The MOKE microscopy as the name suggests is based on the Magneto-Optical Kerr effect, wherein polarized light reflected from a magnetic material undergoes a rotation of its polarization. Measuring the rotation or change of polarization of the reflected beam gives information about the magnetization state of the sample [62]. This rotation depends on the relative orientation of the incident polarization with the sample magnetization. Therefore, the Kerr effect can be classified into longitudinal, transverse, and polar Kerr effect based on the direction of the magnetization vector with respect to the incident and sample planes. The MOKE microscopy is a versatile and well-established technique and is a more simple approach in comparison to the micro-SQUID, as the samples can easily be measured without an additional structure fabrication. Measuring the Kerr signal from a cylindrical nanowire is however a challenging task due to the small probing area available. In addition to this, the curvature of the nanowire further reduces the signal from the probed area, since at a given time only one Kerr effect (say longitudinal Kerr effect wherein the magnetization is in the plane of the sample) is probed. Due to these reasons, it is crucial to achieve a good focus of the laser spot on the nanowire and attain the highest possible alignment of the setup (such as lenses, laser, etc.), in order to obtain a high Kerr signal from the nanowire.

The MOKE measurements of a Ni nanowire yield a magnetic hysteresis loop as depicted in **Figure 10** [41]. The obtained hysteresis loop is characterized by two saturated states indicating opposite directions of magnetization within the nanowire, with a sudden jump in the hysteresis

loop indicating a sharp reversal of the nanowire's magnetization. The magnetic field value at which a sharp reversal of the nanowire magnetization is observed is considered as the switching field (Hsw). The above observations of the magnetization reversal are indicative of a single magnetic domain behavior of the nanowire [41, 63].

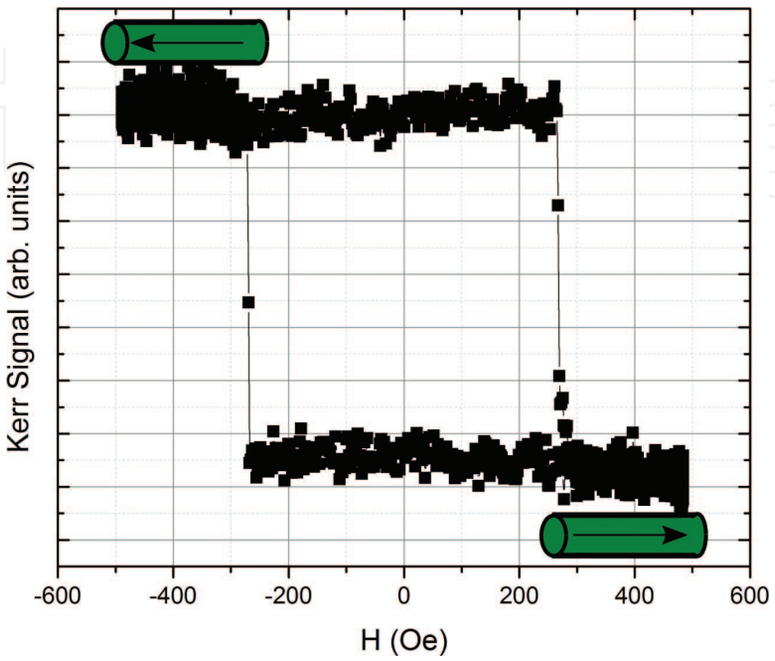

Figure 10. Hysteresis loop of a single Ni nanowire (160 nm diameter and 12 μm in length). The arrows in the schematics indicate the magnetization direction within the nanowire (reprinted from Vilanova Vidal et al. [41], with the permission of AIP publishing).

In addition to obtaining information directly related to the magnetic hysteresis loops of a single nanowire, the magnetization reversal mechanism of the nanowire can be probed by modifying the measurement routine such as by changing the angle of the applied field during the measurement, i.e., angular dependence studies, which would yield the angular nanowire coercivity. Also, the measurement of several individual nanowires and their behavior with fields applied at various angles can be probed in the MOKE [41].

4.2.2. Magnetic imaging

Imaging the magnetic signal of a nanowire and its response to an external magnetic field yields useful information about the nanowire's magnetization reversal process, as well as details of the magnetic domains and domain walls. The versatility of the imaging techniques has increased interest in the study and control of domain-wall dynamics, which is fundamental for domain-wall propagation–based applications. Even though imaging of cylindrical nanowires is relatively straight forward, the interpretation of the obtained data is challenging, as the nanowires are three dimensional unlike in the case of planar structures, thus increasing the complexity of single nanowire characterization. Also, the nanowires' cylindrical shape makes the domain-wall internal structure difficult to visualize, like the core of a vortex domain wall.

Magnetic force microscopy (MFM) is a scanning probe microscopy technique which is widely used for the magnetic imaging of nanostructures [64]. The MFM is a special operational mode of the atomic force microscope (AFM), wherein the standard AFM tip is replaced with a magnetic tip usually coated with a high coercivity thin film to fix the magnetization of the tip during imaging. During an MFM scan, the magnetic tip interacts with the magnetic stray fields near the sample surface, and the strength of the local magnetostatic interaction results in a magnetic map of the scanned area. **Figure 11(a)** depicts the AFM image of a Ni nanowire, whose corresponding MFM images at remanence are depicted in **Figure 11(b ,c)**. Firstly, a magnetic field is applied to saturate the nanowire in a particular direction. When the nanowire is magnetically saturated, a dark and bright signal or spot can be observed at the ends of the nanowire. These spots are a result of the stray fields from the ends of the nanowire, which interact with the MFM tip resulting in a repulsive and attractive interaction. In order to understand the magnetization reversal and determine the switching field of the nanowire, the following procedure is performed: firstly, a magnetic field is applied to saturate the nanowire in a particular direction. The magnetic field is then removed, and the nanowire is imaged at remanence. The scans are performed at remanence in order to avoid effects of the stray field of the MFM tip on the nanowire's switching field. The magnetic field is then increased in the opposite direction, until the magnetization of the nanowire is reversed. MFM studies reveal that the nanowire consists of a single magnetic domain with a sharp transition between the two magnetic states. The magnetic field value for which a change in contrast at the ends of the nanowire is observed is considered as the Hsw of the nanowire. The observations from the MFM images agree with the previously obtained MOKE results (**Figure 10**) and confirm the single domain structure of the nanowire [41].

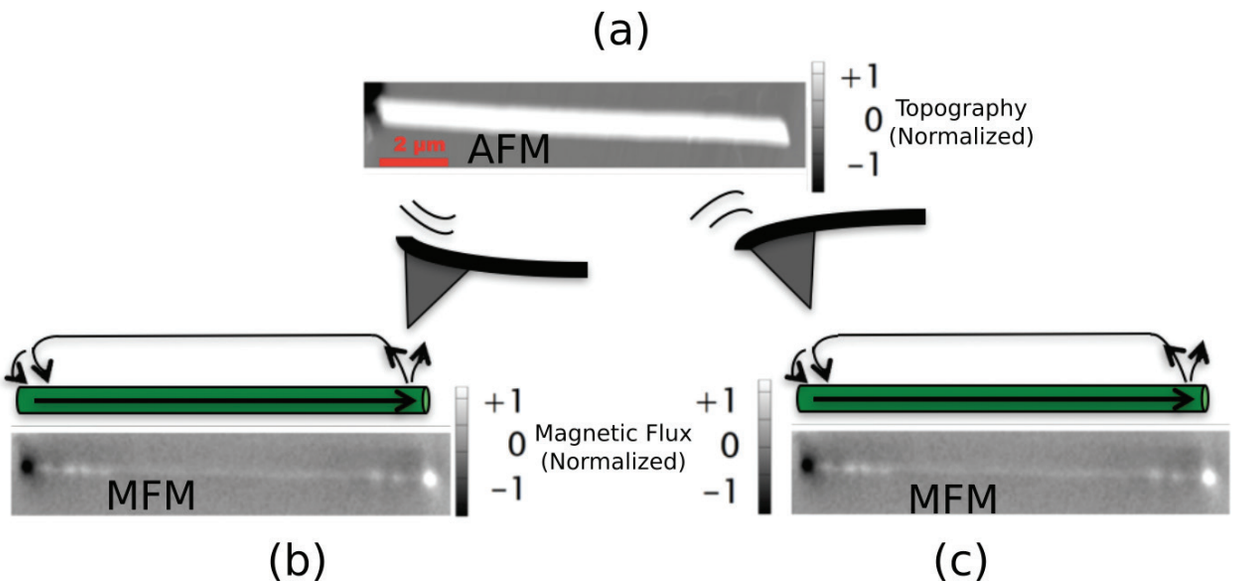

Figure 11. (a) Atomic force microscopy (AFM) image of a Ni nanowire, and (b–c) corresponding magnetic force microscopy (MFM) image of the Ni nanowire. The direction of nanowire magnetization is indicated by the arrows within the nanowire. The interaction of the MFM tip with the nanowire's stray field is depicted as a repulsive and attractive interaction (reprinted from Vilanova Vidal et al. [41], with the permission of AIP publishing).

Several other techniques exist such as Lorentz microscopy [65], modified differential phase contrast microscopy [66], photoemission electron microscopy (PEEM) combined with X-ray magnetic circular dichroism (XMCD) [67, 68], and electron holography [69], which are powerful characterization tools that can yield highly valuable local magnetic information.

4.2.3. Micromagnetic simulations

Even though experimental magnetic characterization techniques offer valuable information about the magnetic nature of the nanowire, they are limited mainly by the 2D data that is obtained as well as the challenges in studying different parameters. Micromagnetic simulation is a versatile tool to understand the magnetization reversal process in nanowires and therefore very useful for interpreting the data obtained from experimental techniques. There are several open source and commercial micromagnetic simulation packages available such as MAGPAR [70], NMag [71], OOMMF [72], LLG Micromagnetics Simulator [73] etc. Studies using micromagnetic simulation tools have revealed that the magnetization reversal in cylindrical nanowires occurs by the nucleation and propagation of domain walls rather than by means of coherent rotation or curling (as was previously understood) and that the type of the domain wall depends on the diameter of the nanowire. As an example, the magnetization reversal process of a polycrystalline Ni (diameter of 160 nm) nanowire was simulated using the MAGPAR package [41]. Since the nanowire consists of a polycrystalline structure, a tetrahedral mesh was randomly assigned with an average mesh size of 6 nm, which is approximately the exchange length of Ni [74]. **Figure 12** gives an overview of the reversal process and consists of four snapshots from the reversal process of the simulated nanowire (green arrows indicate the magnetization direction). Firstly, the nanowire is saturated in the $+M_Z$ direction. The magnetic field is then reduced until remanence after which it is applied in the opposite direction, i.e., $-M_Z$ direction. At remanence, most of the nanowire is magnetized in the $+M_Z$ direction, except for the nanowire ends, which consist of a pair of open vortex areas (OVAs) that are formed as a consequence of the demagnetizing field (to minimize the magnetostatic energy). The magnitude of the magnetic field is increased in the $-M_Z$ direction, and at the switching field, two domain walls (Bloch-point domain walls) nucleate and propagate toward the center of the nanowire, reversing the magnetization direction (Switching process in **Figure 12**). Upon further increase of the magnetic field, the nanowire's magnetization attains a saturated state (saturation state in **Figure 12**).

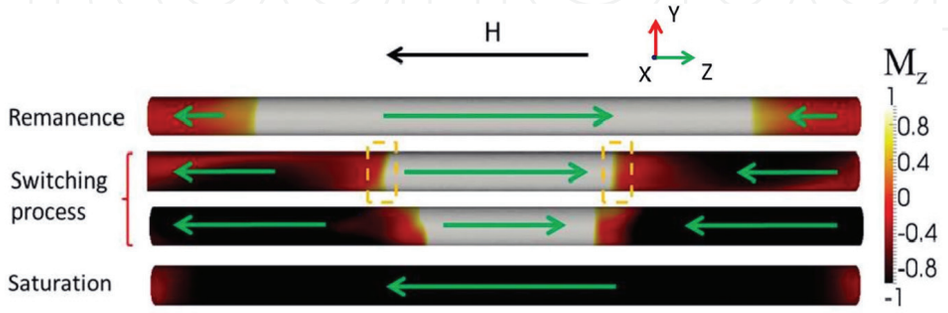

Figure 12. Visualization of the magnetization reversal process from remanence in the +z direction to saturation in the –z direction. The dashed boxes indicate the Bloch-point domain walls (reprinted from Vilanova Vidal et al. [41], with the permission of AIP publishing).

4.2.4. Combination techniques

By utilizing various magnetic characterization techniques (such as magnetometry, magnetic imaging, and micromagnetic simulations) in combination with different measurement routines such as angular dependence studies, it is possible to gain valuable additional information. For example, the effect of the cross-section shape of the nanowire with the switching field (H_{SW}) is investigated using MOKE, MFM, and the Magpar package [41]. The simulations were performed utilizing a circular and a real cross-sectional shape of a nanowire as depicted in **Figure 13(a)** from θ = 0° to 70°. In **Figure 13(b)**, the simulated angular dependencies of the ideal circular and real cross-sections are plotted along with the experimental MOKE and MFM results. It was observed that the values of H_{SW} of nanowires with real and ideal cross-sections

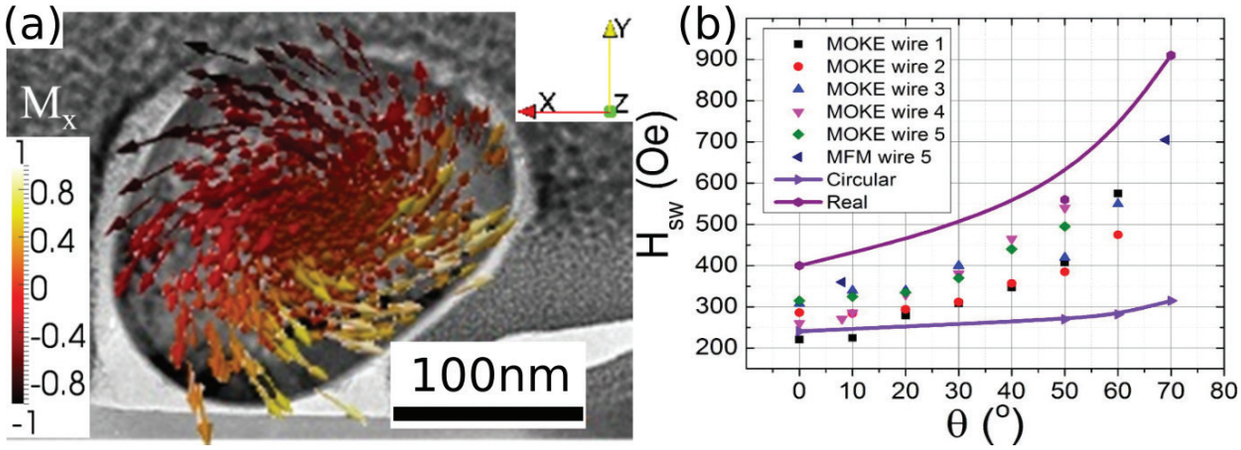

Figure 13. (a) Micromagnetic simulations performed using a real cross-section of a Ni nanowire, (b) dependence of switching field with angle between the nanowire and applied field, of five nickel nanowires measured using MOKE, MFM, and micromagnetic simulations. The simulations were performed using different nanowire cross-section shapes namely circular and real cross-section (reprinted from Vilanova Vidal et al. [41], with the permission of AIP publishing).

are different from each other. For example at θ = 0°, the H_{SW} of ideal cross-section is around 60% of the real cross-section. The angular H_{SW} simulations of the real and circular nanowire cross-section depict two different slopes of the curve. In the real cross-section, increasing angles leads to a higher value of H_{SW}, whereas not much of an increase is observed with increasing angles in the circular cross-section. Interestingly, the H_{SW} values obtained from the circular and real cross-sections define a range inside which all the experimental data fit. This suggests that the different H_{SW} values found for different nanowires are a result of their slightly different cross-sectional shapes. While the simulation with the circular cross-section yields the smallest possible values for H_{SW}, it might be possible to observe even larger values than the ones found for the real cross-section, depending on the actual cross-section shape of the nanowire ends. Thus, the micromagnetic simulations performed here are able to reproduce the experimental scattering obtained for H_{SW} of different nanowires. The cross-sectional shape of the nanowire strongly influences H_{SW}. This is an observation that is particularly relevant from a technological point of view, where the properties of individual nanowires need to be taken into account for device design.

4.3. Electrical characterization

The study of the magnetic and transport properties of cylindrical nanowires such as thermal and resistivity studies, anisotropic magneto resistance, spin transport, etc. is important from a fundamental point of view to investigate unique properties that may arise due to the size of the structures. From a technological perspective, electrical characterization is crucial for device applications. There are several challenges involved in the electrical characterization of a single nanowire such as the contacting of a single nanowire, attaining a low contact resistance, and avoiding electrical discharge that would otherwise result in destroying the nanowire.

4.3.1. In-situ characterization

There are two approaches to electrically address a single nanowire [15, 75–79]. The first approach involves addressing nanowires that are still in the AAO template, i.e., *in-situ* characterization [75, 76]. This is achieved by patterning electrodes on either side of the AAO template, taking care to contact only a single nanowire. The disadvantage of this approach is that the contacted nanowire could be influenced by the neighboring nanowires. Also, it is not possible to analyze the contacted nanowire for the presence of defects or other irregularities which would affect the electrical characterization of the nanowire. In addition to this, the technique is limited to two-point measurement.

4.3.2. Ex-situ characterization

The second approach to electrically address a single nanowire is by contacting released nanowires, i.e., *ex-situ* characterization [15, 76–79]. The advantages of the *ex-situ* approach are that nanowires can be chosen selectively under a microscope, which allows to probe any structural deformities along its length. In this approach, measurements are not limited to two-point geometry, and different sections of the same nanowire (as small as 500 nm) can be probed. An added advantage of the *ex-situ* approach is that several characterization techniques such as MFM and MOKE can be performed on the same nanowire, thus allowing the nanowire's extensive electrical and magnetic characterization [41]. The *ex-situ* characterization can be realized by two methods, by dispersing nanowires onto prefabricated electrodes or by dispersing nanowires onto a substrate (such as Si/SiO_2) and patterning electrodes onto the dispersed nanowire. The former technique requires careful alignment of the nanowires with the electrodes, such as by applying an external magnetic field. The latter does not require any nanowire manipulation but involves the identification of a dispersed nanowire such as by using a scanning electron microscope (SEM) followed by marking its location by patterning alignment marks using a focused ion beam (FIB). Here, it is crucial to obtain sufficiently isolated nanowires which are spread over the substrate. This can be achieved by diluting the nanowire-containing ethanol stock solution to reduce the concentration of dispersed nanowires. The alignment marks aid in electrode placement in the subsequent lithography steps. This approach allows the selection of a nanowire with high precision, as well as contacting only a single nanowire with no additional structures in the vicinity of the nanowire. Generally, the electrode design is patterned either by electron-beam lithography (EBL) [15] or optical lithography [80]. Both the exposure systems have their own advantages and disadvantages. Even though EBL is a labor, cost, and time-intensive process, it

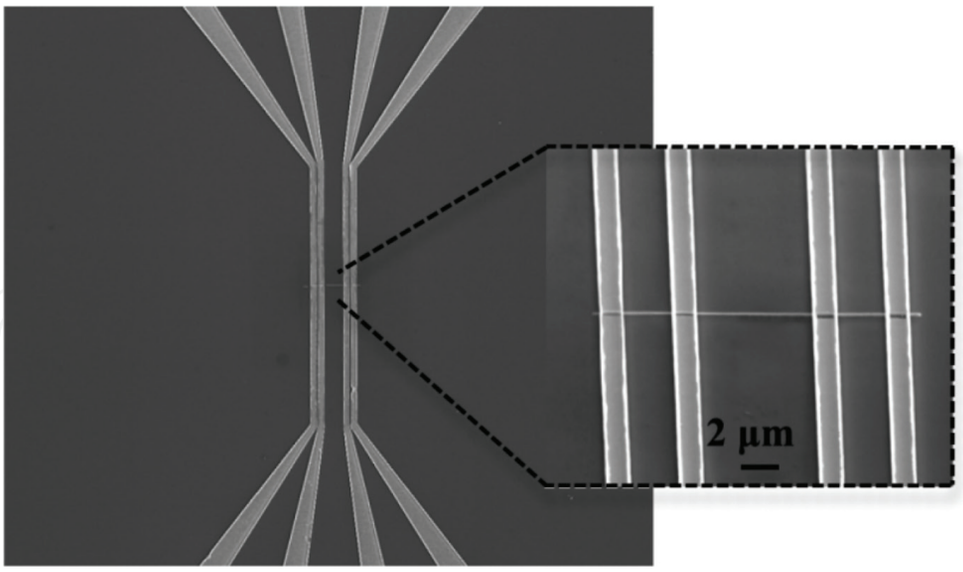

Figure 14. SEM image of electrodes patterned using electron-beam lithography onto a single nanowire. Inset depicts a magnified image (© [2016] IEEE. Reprinted, with permission, from Mohammed et al. [15]).

achieves high precision and small electrode widths (**Figure 14**). This is advantageous when the nanowires are of a shorter length. In the case of EBL, the alignment of the electron beam with the nanowire is extremely challenging especially when it involves a large number of electrodes. Optical lithography on the other hand is a relatively quick process but has limitations regarding the minimum width of electrodes as well as the length of the nanowires that can be used. Once the design is lithographically patterned, electrodes are deposited onto the nanowire. To obtain a good ohmic contact between the electrodes and the nanowire, an etch step is performed prior to the electrode deposition, in order to remove the nanowire oxide layer at the resist openings. This etching process is optimized by systematically controlling the etch time to avoid over or under etching of the nanowire.

4.3.3. Magnetoresistance of individual nanowires

The magnetoresistance (MR) effect has its origin in spin–orbit interaction and depends on the relative orientation of the magnetic moments with respect to the direction of applied electric current. The magnetoresistance (MR) curve offers an insight into the switching behavior of nanowires [81]. **Figure 15(a)** depicts the schematics for MR measurement and (b) shows the magnetization reversal/MR curve of a Ni nanowire (160 nm diameter). At magnetic saturation, the magnetic moments are aligned parallel to the direction of current indicated by the high resistance state in the MR curve. Reversal of the magnetic field results in a decrease of resistance as the magnetic moments continuously rotate away from the direction of current [13, 15, 82]. At a distinct value of the magnetic field referred to as the switching field H_{SW}, there occurs an abrupt reversal of the magnetic moments, which is indicated by a sudden jump of resistance [15], as shown in **Figure 15(b)**.

The MR curve is also useful to identify interruptions in the domain wall motion during the magnetization reversal of the nanowire. These interruptions referred to as pinning can

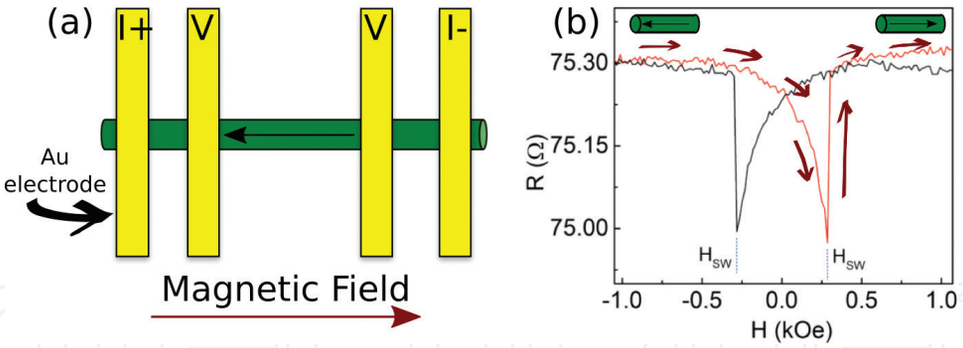

Figure 15. (a) Magnetoresistance measurement schematic depicting a nanowire with four electrodes patterned onto it. The black arrow within the nanowire indicates the nanowire's magnetization direction, (b) Magnetoresistance curve of a Ni nanowire starting from negative saturation to positive saturation (depicted by the red arrows) followed by performing the measurement in the reverse direction, i.e., from positive to negative saturation. The black arrow within the nanowire indicates the nanowire's magnetization direction (reprinted from Vilanova Vidal et al. [41], with the permission of AIP publishing).

be a consequence of a defect (pinning site) within the nanowire. Pinning can be artificially introduced by local modification of magnetic properties by utilizing multisegmented or diameter-modulated nanowires, as well as by introducing notches onto the nanowire. For nanowire-based data storage applications, it is essential to create reliable pinning sites along the nanowire so that domain walls (or bits) can be reliably pinned and depinned (to move the bits) along the nanowire.

Figure 16(a) is an SEM image of a nickel nanowire (20 μm long with a diameter of 160 nm) with four triangular notches patterned onto it using an SEM equipped with a focused ion beam. The MR curve of the notched nanowire constitutes a nonabrupt reversal or a step in the magnetization reversal curve at the H_{SW} (~150 Oe). This discontinuity during the magnetization reversal is an indication of a domain wall which would only depin upon further increase of the applied field. The magnetization reversal at H_{SW} shows two steps (the circles represent the step positions) in **Figure 16(b)**. These two steps are present in both directions and are an indication for domain wall pinning at the two constriction sites.

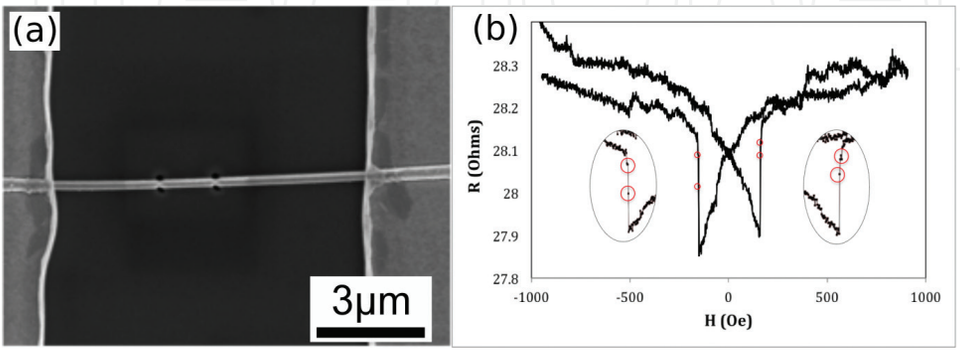

Figure 16. (a) SEM image of a Ni nanowire with notches (to pin domain walls) etched using a focused ion beam, (b) MR curve of the Ni nanowire with notches. Insets depict the magnified area of the MR curve where pinning is observed (represented by the circles).

5. Characterization of multisegmented Co/Ni nanowire

The characterization of multisegmented Co/Ni nanowires (consisting of hcp Co and fcc nickel structure) reveals interesting features. It has been observed that the interface between the Co and the Ni segment act as pinning sites (**Figure 17**). This is an important feature for the application of such nanowires as 3D memory devices.

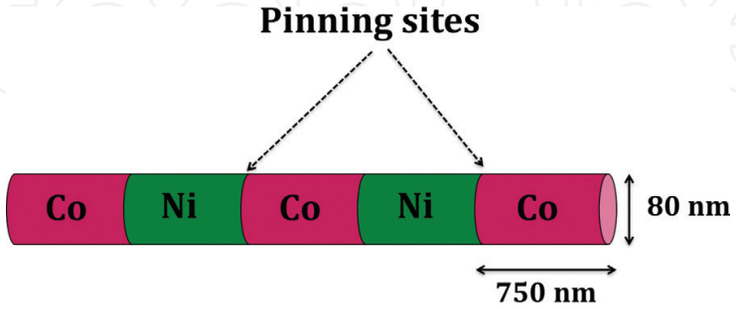

Figure 17. Schematic of a multisegmented nanowire consisting of alternating segments of cobalt and nickel.

Figure 18 depicts the MR curve of a multisegmented Co/Ni nanowire. The magnetization reversal of the nanowire proceeds from a magnetically saturated state indicated by the high resistance value in the MR curve (**Figure 18(a)**). As the direction of applied field is reversed, a gradual decrease in resistance is observed. This decreasing resistance in the MR curve is a consequence of the rotation of the nanowire's magnetic moments away from the direction of applied current. We

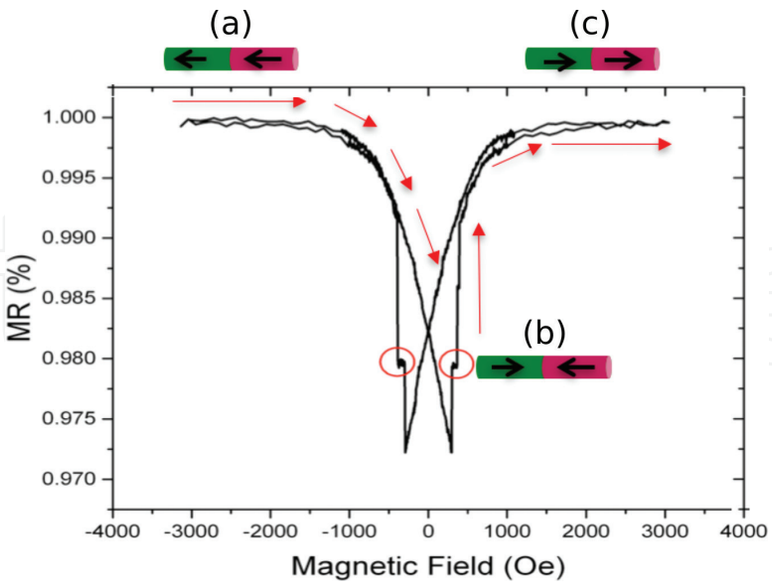

Figure 18. Magnetoresistance curve of a multisegmented co/Ni nanowire. Stage (a) of magnetization reversal depicts the saturated state wherein the magnetic moments are aligned parallel to the current, stage (b) depicts a nanowire with a domain wall (head to head in this case), and finally, stage (c) represents the saturated state with the nanowire having a reversed magnetization direction to that in stage (a). (reprinted (adapted) with permission from Ivanov et al. [83]. Copyright (2017) American Chemical Society).

find that the MR curve of the multisegmented Co/Ni nanowire differs from that of the Ni nanowire in **Figure 15(b)**. Here, the MR curve is similar to the nanowire with notches (**Figure 16(b)**), i.e., instead of the distinct jump at H_{SW}, it displays an interruption or plateau during the jump (**Figure 18(b)**). The plateau indicates that the magnetization does not reverse at once, and magnetization reversal proceeds only upon further increase of the applied magnetic field. This region of the curve is indicative of the pinning of a domain wall, which continues to propagate upon further increase in the magnetic field. Finally, the direction of magnetization within the nanowire is reversed, leading to a parallel alignment of the magnetic moments with respect to the current, which is indicated by the high resistance value in the MR curve (**Figure 18(c)**).

MFM studies performed on the multisegmented Co/Ni nanowire reveal interesting features. As discussed earlier in Section 4.2.2, the MFM image of a single domain state of a nanowire is characterized by a bright and a dark spot at the ends of the nanowire (**Figure 11**). The MFM image of a Co/Ni nanowire with a domain wall pinned at the interface however displays a different stray field configuration. In this case, the contrasts or spots from the ends of the nanowire would be the same, and in addition to this, an alternate contrast would be observed at the interface. **Figure 19** is an MFM image of a multisegmented Co/Ni nanowire and is characterized by two bright spots at the end of the nanowire and a more pronounced black spot at the interface, from which the magnetization state of the nanowire a two domain state with a domain wall pinned at the center can be inferred. The MFM image confirms that the interface in fact acts as a pinning site as indicated by the MR curve.

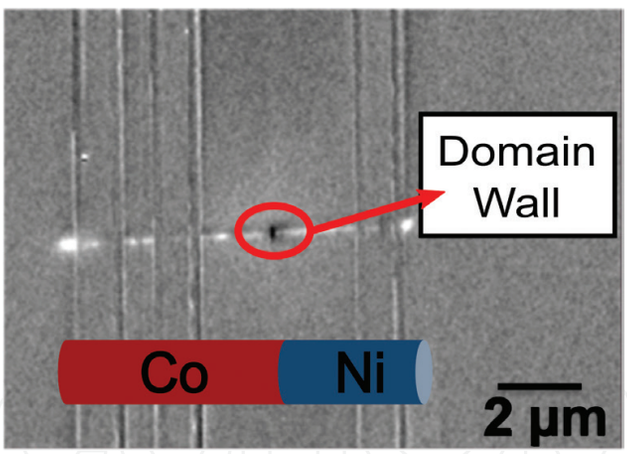

Figure 19. MFM of a multisegmented co/Ni nanowire with a domain wall pinned at the interface. The arrows within the nanowire schematic represents the direction of magnetization within the nanowire (© [2016] IEEE. Reprinted, with permission, from Mohammed et al. [15]).

6. Characterization of diameter modulated nanowires

Nanowires grown in templates allow for the fabrication of nearly one-dimensional structures (see Section 3.2 and 3.3). When the shape of the pores is tailored, e.g., by diameter modulation as described in Section 2.2, the growing nanowires will fill the pores and acquire the geometry of the AAO template (**Figure 20(a)**). From the various experimental and micromagnetic simulation results, general behaviors of the magnetization reversal mechanisms can be found that

relate to the nanowire diameter modulation. The nucleation of a domain wall begins at the free ends and/or at the diameter transition, and the domain wall propagates from the thicker to the thinner segment [84]. Small diameters favor transverse domain walls, due to the exchange interaction contribution, while larger diameters favor vortex domain walls, where longer range dipolar interaction becomes more relevant [85]. This means H_{SW} values are dominated by the segment of larger diameter and explain why small differences in diameter between the two ends of a nanowire promote the propagation of a domain wall from only one end. Also, the dipolar interaction between segments with different diameters reduces the switching and saturation fields compared to a conventional nonmodulated nanowire with diameter equal to the thinner segment [16, 32, 84]. This is due to the strong interaction between the stray fields at the ends of each segment which is a result of the sudden diameter change. Domain walls can nucleate at these perpendicular surfaces as a mechanism to minimize the magnetostatic energy [86].

Figure 20(b) shows an AFM image of a FeCoCu nanowire with the diameter modulated between 100 and 140 nm. As seen in the MFM image of **Figure 20(c)**, the single domain configuration of the nanowire is maintained independent of the number of modulations. Stray fields are emanating not only from the ends of the nanowire, as in the case of nanowires with constant diameter (**Figure 11(b**,**c)**) but also from the ends of the segments with larger diameters [29, 88].

Modulations of the magnetization profile lead to the creation of pinning sites for domain walls [37, 87]. Magnetic poles of different signs are created at the modulation transition regions,

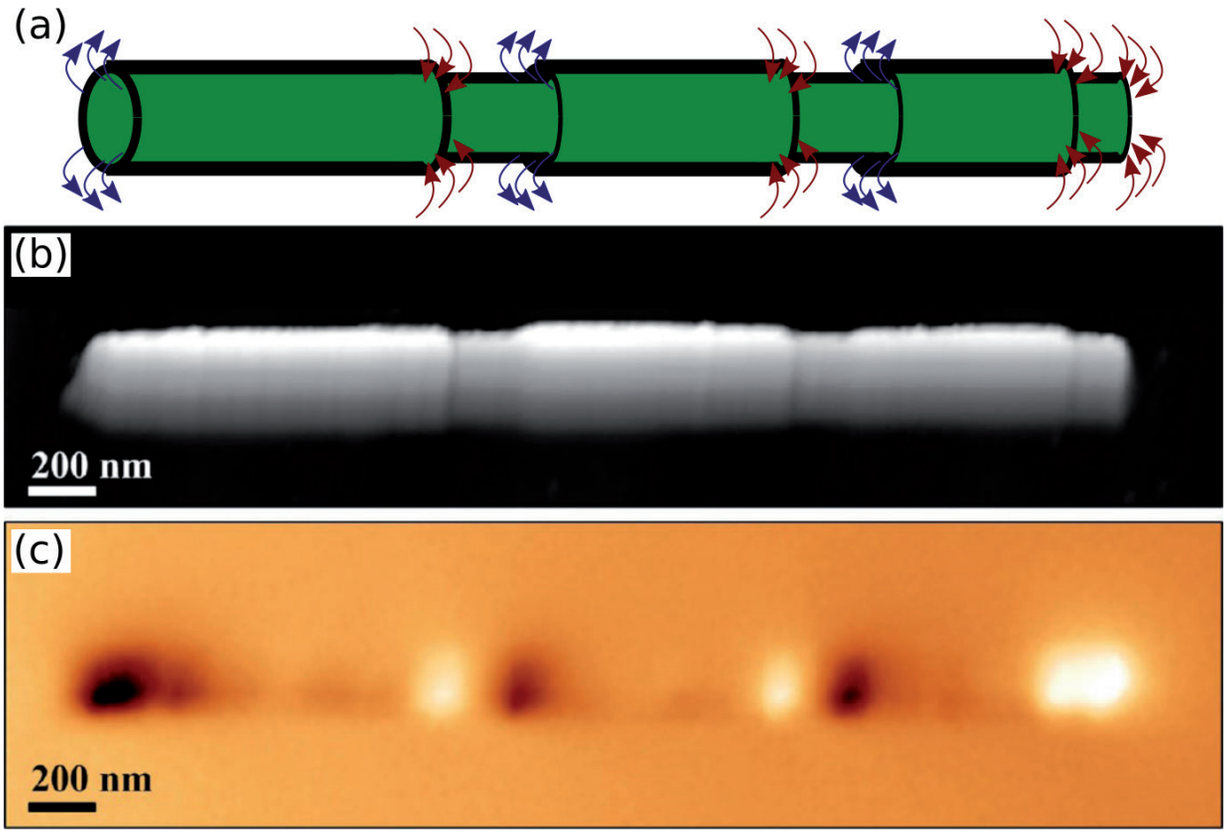

Figure 20. (a) Schematic of a diameter-modulated nanowire. (b) AFM image and (c) corresponding MFM image of a diameter-modulated FeCoCu nanowire (reprinted with permission from Rodríguez et al. [87]. Copyright 2016 American Chemical Society).

increasing the magnetic surface charge, which is minimized by the creation of vortex states. The efficiency of domain wall pinning sites in cylindrical nanowires depends on the parameters that modify the magnetization profile with respect to the magnetic surface charges. Hence, the pinning sites' geometrical magnetizations can be used to tailor the properties of cylindrical nanowires and integrate different functionalities into them.

7. Characterization of core-shell Fe-Fe_3O_4 nanowires

Energy-filtered transmission electron microscopy (EF-TEM) can be used to study the evolution of the core-shell nanowire structure for different oxidation times. TEM studies into core-shell Fe-Fe_3O_4 nanowires have revealed that annealing of both polycrystalline or single-crystal iron nanowires leads to the formation of an oxide shell structure (**Figure 21(a)**) but possess distinctly different characteristics [50]. The oxide shell thickness of polycrystalline Fe nanowires (**Figure 21(b,c)**) increases linearly with annealing time until the disappearance of the Fe core, leaving behind a pure Fe_3O_4 nanowire. However, the oxidation of the single-crystal Fe nanowires (**Figure 21(d,e)**) is observed to be a slower process, and the shell thickness does not increase beyond a certain limit (12 nm), thus maintaining the Fe core structure. It was observed that the O clearly concentrates at the edges while in fully oxidized nanowires; O is distributed across the entire volume. This can be attributed to the absence of grain boundaries that are required for heat-assisted oxygen diffusion. The ability of single-crystal core-shell nanowires to resist complete oxidation is a great advantage for applications that require high-temperature operations, while they maintain the magnetic properties of the Fe core [50].

Magnetic force microscopy studies into polycrystalline and single-crystal core-shell Fe-Fe_3O_4 nanowires reveal marked differences. The single-crystal Fe and the core-shell nanowires fabricated from single-crystal Fe displays a single magnetic domain state, whereas a multidomain state is observed in core-shell nanowires fabricated from polycrystalline Fe nanowires.

The core-shell nanowire is an attractive candidate for biomedical applications [7, 8, 83], due to their tunable magnetization and long-term stability. In addition to this, a high degree of

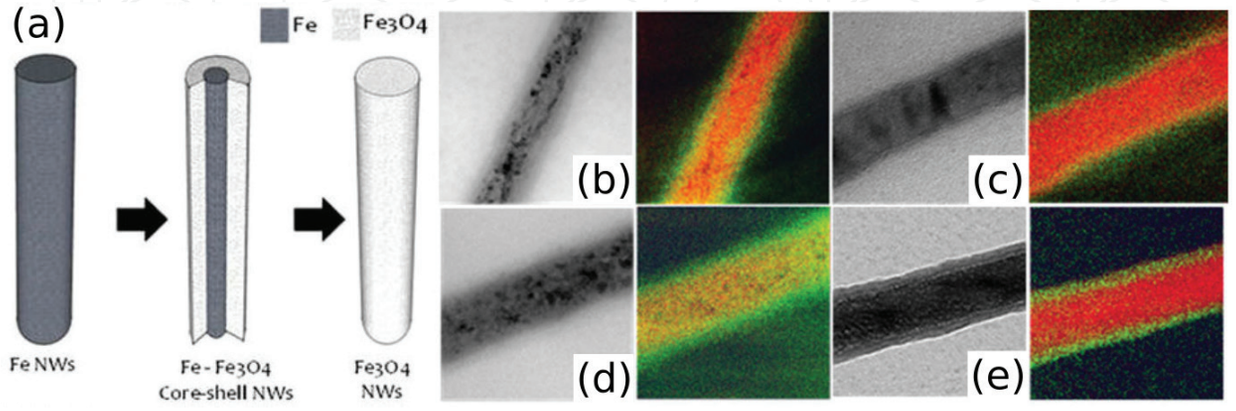

Figure 21. (a) Formation of the Fe-Fe_3O_4 core-shell structure, (b–e) bright field color-coded EF-TEM images of the Fe (red) and O (green) of polycrystalline Fe nanowires after (b) 20 min, (c) 24 h annealing and single crystalline Fe nanowires after (d) 1 h, (e) 72 h [50].

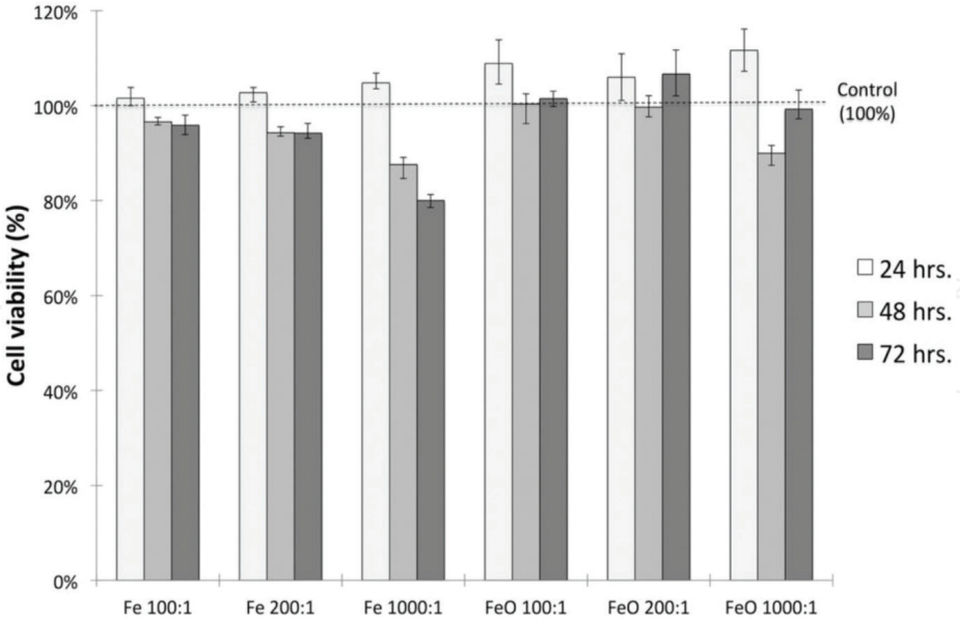

Figure 22. Cell viability studies of colon cancer cells incubated with Fe and Fe-Fe_3O_4 core-shell nanowires with varying concentrations (nanowire-to- cell ratio) for 24, 48, and 72 h [50].

biocompatibility required for biomedical applications has been demonstrated by these nanowires. For instance, studies into the metabolic activity of cells incubated with Fe and Fe-Fe_3O_4 core-shell nanowires of varying concentrations and incubation times (**Figure 22**) reveal that the nanowires have comparable and high values of cell viability at concentration of 100 and 200 nanowires per cell. At very high concentrations of 1000 nanowires per cell, Fe nanowires cause a decrease in cell viability to about 80% after 72 h, while viability with Fe-Fe_3O_4 core-shell nanowires remains high.

Author details

Hanan Mohammed, Julian A. Moreno and Jürgen Kosel*

*Address all correspondence to: jurgen.kosel@kaust.edu.sa

King Abdullah University of Science and Technology, Thuwal, Saudi Arabia

References

[1] Alfadhel A, Li B, Zaher A, Yassine O, Kosel J. A magnetic nanocomposite for biomimetic flow sensing. Lab on a Chip. 2014;**14**:4362-4369

[2] Fratila RM, Rivera-Fernández S, Jesús M. Shape matters: Synthesis and biomedical applications of high aspect ratio magnetic nanomaterials. Nanoscale. 2015;**7**:8233-8260

[3] Alfadhel A, Kosel J. Magnetic nanocomposite cilia tactile sensor. Advanced Materials. 2015;**27**:7888-7892

[4] Alnassar M, Alfadhel A, Ivanov YP, Kosel J. Magnetoelectric polymer nanocomposite for flexible electronics. Journal of Applied Physics. 2015;**117**:17D711

[5] Contreras MF, Sougrat R, Zaher A, Ravasi T, Kosel J. Non-chemotoxic induction of cancer cell death using magnetic nanowires. International Journal of Nanomedicine. 2015;**10**:2141

[6] Yassine O, Zaher A, Li EQ, Alfadhel A, Perez JE, Kavaldzhiev M, et al. Highly efficient thermoresponsive nanocomposite for controlled release applications. Scientific Reports. 2016;**6**:28539

[7] Martínez-Banderas AI, Aires A, Teran FJ, Perez JE, Cadenas JF, Alsharif N, et al. Functionalized magnetic nanowires for chemical and magneto-mechanical induction of cancer cell death. Scientific Reports. 2016;**6**:35786

[8] Shore D, Pailloux SL, Zhang J, Gage T, Flannigan DJ, Garwood M, et al. Electrodeposited Fe and Fe-Au nanowires as MRI contrast agents. Chemical Communications. 2016; **52**:12634-12637

[9] García-Martín J, Thiaville A, Miltat J, Okuno T, Vila L, Piraux L. Imaging magnetic vortices by magnetic force microscopy: Experiments and modelling. Journal of Physics D: Applied Physics. 2004;**37**:965

[10] Piraux L, George J, Despres J, Leroy C, Ferain E, Legras R, et al. Giant magnetoresistance in magnetic multilayered nanowires. Applied Physics Letters. 1994;**65**:2484-2486

[11] Piraux L, Renard K, Guillemet R, Mátéfi-Tempfli S, Mátéfi-Tempfli M, Antohe VA, et al. Template-grown NiFe/Cu/NiFe nanowires for spin transfer devices. Nano Letters. 2007;**7**:2563-2567

[12] Wang Z, Kuok M, Ng S, Lockwood D, Cottam M, Nielsch K, et al. Spin-wave quantization in ferromagnetic nickel nanowires. Physical Review Letters. 2002;**89**:027201

[13] Wernsdorfer W, Hasselbach K, Benoit A, Barbara B, Doudin B, Meier J, et al. Measurements of magnetization switching in individual nickel nanowires. Physical Review B. 1997;**55**:11552

[14] Kou X, Fan X, Dumas RK, Lu Q, Zhang Y, Zhu H, et al. Memory effect in magnetic nanowire arrays. Advanced Materials. 2011;**23**:1393-1397

[15] Mohammed H, Vidal EV, Ivanov YP, Kosel J. Magnetotransport measurements of domain wall propagation in individual multisegmented cylindrical nanowires. IEEE Transactions on Magnetics. 2016;**52**:1-5

[16] Whitney T, Jiang J, Searson P, Chien C. Fabrication and magnetic properties of arrays of metallic nanowires. Science. 1993;**261**:1316-1320

[17] Metzger RM, Konovalov VV, Sun M, Xu T, Zangari G, Xu B, et al. Magnetic nanowires in hexagonally ordered pores of alumina. IEEE Transactions on Magnetics. 2000;**36**:30-35

[18] Nielsch K, Müller F, Li A-P, Gösele U. Uniform nickel deposition into ordered alumina pores by pulsed electrodeposition. Advanced Materials. 2000;**12**:582-586

[19] Pitzschel K, Bachmann J, Martens S, Montero-Moreno JM, Kimling J, Meier G, et al. Magnetic reversal of cylindrical nickel nanowires with modulated diameters. Journal of Applied Physics. 2011;**109**:033907

[20] Sulka GD, Brzózka A, Liu L. Fabrication of diameter-modulated and ultrathin porous nanowires in anodic aluminum oxide templates. Electrochimica Acta. 2011;**56**:4972-4979

[21] Masuda H, Fukuda K. Ordered metal nanohole arrays made by a two-step replication of honeycomb structures of anodic alumina. Science. 1995;**268**:1466

[22] Lee W, Park S-J. Porous anodic aluminum oxide: Anodization and templated synthesis of functional nanostructures. Chemical Reviews. 2014;**114**:7487-7556

[23] Nielsch K, Hertel R, Wehrspohn R, Barthel J, Kirschner J, Gosele U, et al. Switching behavior of single nanowires inside dense nickel nanowire arrays. IEEE Transactions on Magnetics. 2002;**38**:2571-2573

[24] Sulka GD. Highly ordered anodic porous alumina formation by self-organized anodizing. Nanostructured Materials in Electrochemistry. 2008;**1**:1-116

[25] Kartopu G, Yalçın O. Fabrication and applications of metal nanowire arrays electrodeposited in ordered porous templates. In: Electrodeposited Nanowires and Their Applications. InTech; 2010

[26] Jaafar M, Navas D, Hernández-Vélez M, Baldonedo J, Vázquez M, Asenjo A. Nanoporous alumina membrane prepared by nanoindentation and anodic oxidation. Surface Science. 2009;**603**:3155-3159

[27] Masuda H, Kanezawa K, Nishio K. Fabrication of ideally ordered nanohole arrays in anodic porous alumina based on nanoindentation using scanning probe microscope. Chemistry Letters. 2002;**31**:1218-1219

[28] Liu C, Datta A, Wang Y. Ordered anodic alumina nanochannels on focused-ion-beam-prepatterned aluminum surfaces. Applied Physics Letters. 2001;**78**:120-122

[29] Choi J, Nielsch K, Reiche M, Wehrspohn R, Gösele U. Fabrication of monodomain alumina pore arrays with an interpore distance smaller than the lattice constant of the imprint stamp. Journal of Vacuum Science & Technology, B: Microelectronics and Nanometer Structures: Processing, Measurement, and Phenomena. 2003;**21**:763-766

[30] Maqableh MM, Tan L, Huang X, Cobian R, Norby G, Victora R, et al. CPP GMR through nanowires. IEEE Transactions on Magnetics. 2012;**48**:1744-1750

[31] Sung S-Y, Maqableh MM, Huang X, Reddy KSM, Victora R, Stadler BJ. Metallic 10 nm diameter magnetic sensors and large-scale ordered arrays. IEEE Transactions on Magnetics. 2014;**50**:1-5

[32] Iglesias-Freire Ó, Bran C, Berganza E, Mínguez-Bacho I, Magén C, Vázquez M, et al. Spin configuration in isolated FeCoCu nanowires modulated in diameter. Nanotechnology. 2015;**26**:395702

[33] Minguez-Bacho I, Rodriguez-López S, Vázquez M, Hernández-Vélez M, Nielsch K. Electrochemical synthesis and magnetic characterization of periodically modulated Co nanowires. Nanotechnology. 2014;**25**:145301

[34] Woo L, Ji R, Gösele U, Nielsch K. Fast fabrication of long-range ordered porous alumina membranes by hard anodization. Nature Materials. 2006;**5**:741

[35] Parkhutik V, Shershulsky V. Theoretical modelling of porous oxide growth on aluminium. Journal of Physics D: Applied Physics. 1992;**25**:1258

[36] Lee W, Schwirn K, Steinhart M, Pippel E, Scholz R, Gösele U. Structural engineering of nanoporous anodic aluminium oxide by pulse anodization of aluminium. Nature Nanotechnology. 2008;**3**:234-239

[37] Losic D, Lillo M. Porous alumina with shaped pore geometries and complex pore architectures fabricated by cyclic anodization. Small. 2009;**5**:1392-1397

[38] Salem MS, Sergelius P, Corona RM, Escrig J, Görlitz D, Nielsch K. Magnetic properties of cylindrical diameter modulated Ni80Fe20 nanowires: Interaction and coercive fields. Nanoscale. 2013;**5**:3941-3947

[39] Mohler JB, Sedusky HJ. Electroplating for the Metallurgist, Engineer, and Chemist. Chemical Publishing Company; New York. 1951

[40] Sousa C, Leitao D, Proenca M, Apolinario A, Correia J, Ventura J, et al. Tunning pore filling of anodic alumina templates by accurate control of the bottom barrier layer thickness. Nanotechnology. 2011;**22**:315602

[41] Vilanova Vidal E, Ivanov YP, Mohammed H, Kosel J. A detailed study of magnetization reversal in individual Ni nanowires. Applied Physics Letters. 2015;**106**:032403

[42] Ivanov YP, Chuvilin A, Lopatin S, Kosel J. Modulated magnetic nanowires for controlling domain wall motion: Toward 3D magnetic memories. ACS Nano. 2016;**10**:5326-5332

[43] Özkale B, Shamsudhin N, Chatzipirpiridis G, Hoop M, Gramm F, Chen X, et al. Multisegmented FeCo/Cu nanowires: electrosynthesis, characterization, and magnetic control of biomolecule desorption. ACS Applied Materials & Interfaces. 2015;**7**:7389-7396

[44] Sharma A, Zhu Y, Thor S, Zhou F, Stadler B, Hubel A. Magnetic barcode nanowires for osteosarcoma cell control, detection and separation. IEEE Transactions on Magnetics. 2013;**49**:453-456

[45] Liu K, Nagodawithana K, Searson P, Chien C. Perpendicular giant magnetoresistance of multilayered Co/Cu nanowires. Physical Review B. 1995;**51**:7381

[46] Yahalom J, Tessier D, Timsit R, Rosenfeld A, Mitchell D, Robinson P. Structure of composition-modulated Cu/Ni thin films prepared by electrodeposition. Journal of Materials Research. 1989;**4**:755-758

[47] Palmero EM, Béron F, Bran C, del Real RP, Vázquez M. Magnetic interactions in compositionally modulated nanowire arrays. Nanotechnology. 2016;**27**:435705

[48] Moreno JA. Multi-Segmented Magnetic Nanowires Fabrication and Characterization. King Abdullah University of Science and Technology. Thuwal, Makkah, Saudi Arabia. 2016

[49] Armelles G, Cebollada A, García-Martín A, Montero-Moreno J, Waleczek M, Nielsch K. Magneto-optical properties of core–shell magneto-plasmonic Au-$Co_xFe_{3-x}O_4$ nanowires. Langmuir. 2012;**28**:9127-9130

[50] Ivanov YP, Alfadhel A, Alnassar M, Perez JE, Vazquez M, Chuvilin A, et al. Tunable magnetic nanowires for biomedical and harsh environment applications. Scientific Reports. 2016;**6**:24189

[51] Ovejero JG, Bran C, Vilanova E, Kosel J, Morales MP, Vazquez M. Electrochemical synthesis of core-shell magnetic nanowires. Journal of Magnetism and Magnetic Materials. 2015;**389**:144-147

[52] Ozel T, Bourret GR, Mirkin CA. Coaxial lithography. Nature Nanotechnology. 2015 May 1;**10**(4):319-24

[53] Mayer B, Rudolph D, Schnell J, Morkötter S, Winnerl J, Treu J, et al. Lasing from individual GaAs-AlGaAs core-shell nanowires up to room temperature. Nature Communications. 2013;**4**:2931

[54] Vivas L, Ivanov YP, Trabada D, Proenca M, Chubykalo-Fesenko O, Vázquez M. Magnetic properties of Co nanopillar arrays prepared from alumina templates. Nanotechnology. 2013;**24**:105703

[55] Asenjo A, Jaafar M, Navas D, Vázquez M. Quantitative magnetic force microscopy analysis of the magnetization process in nanowire arrays. Journal of Applied Physics. 2006;**100**:023909

[56] Dubois S, Colin J, Duvail J, Piraux L. Evidence for strong magnetoelastic effects in Ni nanowires embedded in polycarbonate membranes. Physical Review B. 2000;**61**:14315

[57] Li A, Müller F, Birner A, Nielsch K, Gösele U. Polycrystalline nanopore arrays with hexagonal ordering on aluminum. Journal of Vacuum Science & Technology, A: Vacuum, Surfaces, and Films. 1999;**17**:1428-1431

[58] Williams DB, Carter CB, Veyssiere P. Transmission Electron Microscopy: A Textbook for Materials Science. Vol. 10. Springer. New York; 1998

[59] Zhang J, Ma H, Zhang S, Zhang H, Deng X, Lan Q, et al. Nanoscale characterisation and magnetic properties of Co81Cu19/Cu multilayer nanowires. Journal of Materials Chemistry C. 2015;**3**:85-93

[60] Egerton RF. Electron Energy-Loss Spectroscopy in the Electron Microscope. Springer Science & Business Media; 2011

[61] Pignard S, Goglio G, Radulescu A, Piraux L, Dubois S, Declemy A, et al. Study of the magnetization reversal in individual nickel nanowires. Journal of Applied Physics. 2000;**87**:824-829

[62] Tiwari U, Ghosh R, Sen P. Theory of magneto-optic Kerr effects. Physical Review B. 1994;**49**:2159

[63] Hertel R, Kirschner J. Magnetization reversal dynamics in nickel nanowires. Physica B: Condensed Matter. 2004;**343**:206-210

[64] Rugar D, Mamin H, Guethner P, Lambert S, Stern J, McFadyen I, et al. Magnetic force microscopy: General principles and application to longitudinal recording media. Journal of Applied Physics. 1990;**68**:1169-1183

[65] Lopatin S, Ivanov YP, Kosel J, Chuvilin A. Multiscale differential phase contrast analysis with a unitary detector. Ultramicroscopy. 2016;**162**:74-81

[66] Ivanov YP, Lopatin S, Kosel J, Chuvilin A. Unitary detector DPC imaging with multi-scale capabilities for analysis of local magnetic field of nanomaterials. Microscopy and Microanalysis. 2016;**22**:1704-1705

[67] Da Col S, Jamet S, Rougemaille N, Locatelli A, Mentes TO, Burgos BS, et al. Observation of Bloch-point domain walls in cylindrical magnetic nanowires. Physical Review B. 2014;**89**:180405

[68] Kimling J, Kronast F, Martens S, Böhnert T, Martens M, Herrero-Albillos J, et al. Photoemission electron microscopy of three-dimensional magnetization configurations in core-shell nanostructures. Physical Review B. 2011;**84**:174406

[69] Akhtari-Zavareh A, Carignan L, Yelon A, Ménard D, Kasama T, Herring R, et al. Off-axis electron holography of ferromagnetic multilayer nanowires. Journal of Applied Physics. 2014;**116**:023902

[70] Scholz W, Fidler J, Schrefl T, Suess D, Forster H, Tsiantos V. Scalable parallel micromagnetic solvers for magnetic nanostructures. Computational Materials Science. 2003;**28**:366-383

[71] Fischbacher T, Franchin M, Bordignon G, Fangohr H. A systematic approach to multiphysics extensions of finite-element-based micromagnetic simulations: Nmag. IEEE Transactions on Magnetics. 2007;**43**:2896-2898

[72] Donahue M, Porter D. The Object Oriented Micromagnetic Framework (OOMMF) Project at ITL/NIST The OOMMF code is available at http://math.nist.gov/oommf 1998

[73] Scheinfein, M. R. LLG Micromagnetic SimulatorTM (http://llgmicro.home.mindspring.com)

[74] Tannous C, Gieraltowski J. The Stoner-Wohlfarth model of ferromagnetism. European Journal of Physics. 2008;**29**:475

[75] Fusil S, Piraux L, Mátéfi-Tempfli S, Mátéfi-Tempfli M, Michotte S, Saul C, et al. Nanolithography based contacting method for electrical measurements on single template synthesized nanowires. Nanotechnology. 2005;**16**:2936

[76] Fert A, Piraux L. Magnetic nanowires. Journal of Magnetism and Magnetic Materials. 1999;**200**:338-358

[77] Vila L, Piraux L, George J, Faini G. Multiprobe magnetoresistance measurements on isolated magnetic nanowires. Applied Physics Letters. 2002;**80**:3805-3807

[78] Toimil Molares ME, Höhberger EM, Schaeflein C, Blick RH, Neumann R, Trautmann C. Electrical characterization of electrochemically grown single copper nanowires. Applied Physics Letters. 2003;**82**:2139-2141

[79] Tanase M, Silevitch D, Chien C, Reich D. Magnetotransport properties of bent ferromagnetic nanowires. Journal of Applied Physics. 2003;**93**:7616-7618

[80] Mohammed H, Corte-León H, Ivanov Y, Moreno J, Kazakova O, Kosel J. Angular magnetoresistance of nanowires with alternating cobalt and nickel segments. IEEE Transactions on Magnetics. 2017

[81] Wegrowe J, Kelly D, Franck A, Gilbert S, Ansermet J-P. Magnetoresistance of ferromagnetic nanowires. Physical Review Letters. 1999;**82**:3681

[82] McGuire T, Potter R. Anisotropic magnetoresistance in ferromagnetic 3D alloys. IEEE Transactions on Magnetics. 1975;**11**:1018-1038

[83] Ivanov YP, Chuvilin A, Lopatin S, Mohammed H, Kosel J. Direct observation of current-induced motion of a 3D vortex domain wall in cylindrical nanowires. ACS Applied Materials & Interfaces. 2017;**9**(20):16741-16744. DOI: 10.1021/acsami.7b03404

[84] Tejo F, Vidal-Silva N, Espejo A, Escrig J. Angular dependence of the magnetic properties of cylindrical diameter modulated Ni80Fe20 nanowires. Journal of Applied Physics. 2014;**115**:17D136

[85] Wieser R, Nowak U, Usadel K-D. Domain wall mobility in nanowires: Transverse versus vortex walls. Physical Review B. 2004;**69**:064401

[86] Pitzschel K, Moreno JMM, Escrig J, Albrecht O, Nielsch K, Bachmann J. Controlled introduction of diameter modulations in arrayed magnetic iron oxide nanotubes. ACS Nano. 2009;**3**:3463-3468

[87] Rodríguez LA, Bran C, Reyes D, Berganza E, Vázquez M, Gatel C, et al. Quantitative nanoscale magnetic study of isolated diameter-modulated FeCoCu nanowires. ACS Nano. 2016;**10**:9669-9678

[88] Berganza E, Bran C, Jaafar M, Vázquez M, Asenjo A. Domain wall pinning in FeCoCu bamboo-like nanowires. Scientific Reports. 2016;**6**:29702

IntechOpen